COMMUNICATION

Crinkling Ultralong Carbon Nanotubes into Serpentines by a Controlled Landing Process

By *Yagang Yao, Xiaochuan Dai, Chaoqun Feng, Jin Zhang,* Xuelei Liang, Li Ding, Wonmook Choi, Jae-Young Choi,* Jong Min Kim,* and *Zhongfan Liu**

Arrays of carbon nanotubes (CNTs) with identical chirality have significant applications in nanodevices.[1–3] At present, however, neither the chirality-selective growth of CNTs nor post-treatment to separate CNTs with specific chirality is mature enough to achieve uniform chirality.[4–16] Instead, only a narrow distribution of diameter and chirality is achieved. Growth of serpentine CNTs, that is, CNTs with periodic parallel segments of identical chirality and periodic curves between those segments along one ultralong CNT, is thought to be a direct way to form such arrays. Several research groups have made great efforts to synthesize serpentine CNTs,[17,18] however, there is currently little understanding of the detailed growth mechanism and how the growth parameters influence the geometry of the serpentine CNTs, for example, the amplitudes and periods of the serpentine curves. In the work reported here, we have developed a rational method to crinkle ultralong CNTs into serpentine geometries controllably. Based on this method, the yield of serpentine CNTs exceeds 96%, with the amplitudes and density over 100 μm and 2 CNTs μm^{-1}, respectively. Several experimental parameters have also been investigated and the growth mechanism has been further clarified in the meantime. Moreover, the serpentine CNTs are able to be introduced into ultrahigh-current CNT-based devices. Without losing the high on/off ratio that a single CNT exhibits, the current can be easily scaled up if more parallel segments are fabricated into the devices. This growth method of serpentine CNTs smoothes the approach to single-chirality CNT arrays as well as desirable devices based on them and will broaden CNT application to various nanodevices.

Until now, a "falling spaghetti" mechanism has been used to tentatively explain the formation of serpentine CNTs on quartz or sapphire.[17] According to this mechanism, the CNTs are first catalytically synthesized while floating upon the substrate and then absorbed onto the surface in a zigzag pattern from base to tip. As shown in Figure 1a, two forces, the lattice-alignment force (F_r) and the shear friction force (F_u), compete to determine the geometry of the serpentine CNTs. When the CNT lands, the anisotropic quartz surface will preferentially absorb the CNT along its lattice direction, because of the absorption energy difference, which results in a lattice-alignment force F_r. On the other hand, the shear friction force F_u between the flowing gas and the floating portion of the CNT tends to drag it straight forward. The fluctuation of the relative strength of these two forces causes the serpentine geometry of the CNTs.

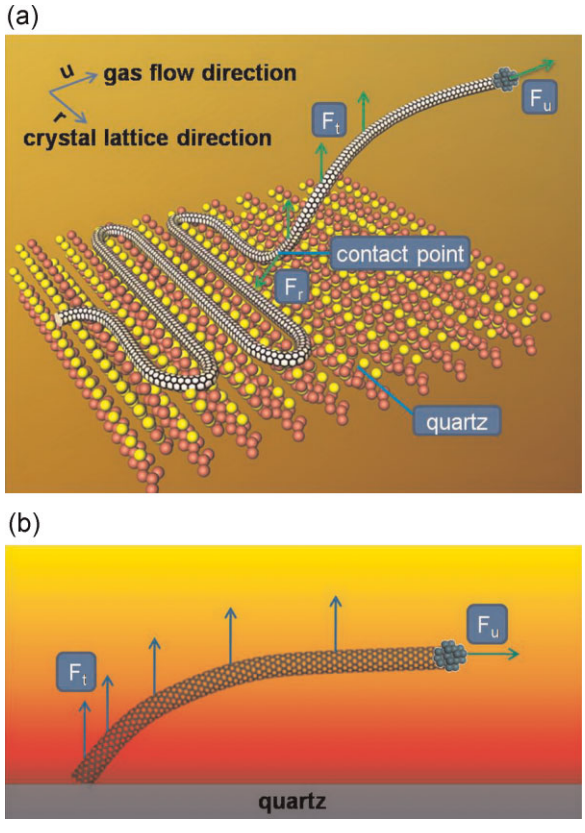

Figure 1. The growth mechanism of serpentine CNTs. a) Competition between the lattice-alignment force F_r and the shear-friction force F_u at the contact point. b) Side elevation of the floating part of an ultralong CNT. The thermal buoyancy force F_t works against gravity to keep the CNT from falling and is crucial in controlled-landing growth.

[*] Prof. J. Zhang, Prof. Z. F. Liu, Y. G. Yao, X. C. Dai, C. Q. Feng
Beijing National Laboratory for Molecular Sciences
Key Laboratory for the Physics and Chemistry of Nanodevices
State Key Laboratory for Structural Chemistry of Unstable and Stable Species
College of Chemistry and Molecular Engineering
Peking University, Beijing 100871 (PR China)
E-mail: jinzhang@pku.edu.cn; zfliu@pku.edu.cn
Dr. J.-Y. Choi, Dr. W. Choi, Dr. J. M. Kim
Samsung Advanced Institute of Technology
San 14-1, Nongseo-Dong, Giheung-Gu, Yongin
Gyeonggi-Do 446-712 (Republic of Korea)
E-mail: jaeyoung88.choi@samsung.com
Prof. X. L. Liang, L. Ding
Key Laboratory for the Physics and Chemistry of Nanodevices
Department of Electronics
Peking University, Beijing 100871 (PR China)

DOI: 10.1002/adma.200901255

By carefully looking into this mechanism and the nature of the forces, we realized that F_r works only on a small portion of CNT, that near to the substrate. This portion should satisfy two conditions: it must be in the force range of the lattice (on the order of nanometers) and not aligned along the lattice already. Imagine the situation that the floating straight CNT is forced to land on the substrate instantly; it is impossible for F_r to curl up the CNT. Therefore, it is important to control the landing process in a gradual and slow manner to allow the competition between the lattice-alignment force and the shear-friction force to act successively on every portion of the CNT during the landing process. To do so, the force keeping CNTs floating, acting against gravity, was analyzed. As shown in Figure 1b, it originates from an upward gas flow due to the heating of the substrate. This thermal buoyancy force F_t[19–21] can be modulated by changing the temperature of the hot zone of the furnace. Because the gas-directed growth mode[22] can be realized at 975 °C but not at 775 °C, it is reasonable to assume that F_t is sufficient to support CNTs at 975 °C but not at 775 °C. Therefore, we designed a gradual cooling step from 975 °C to 775 °C at ultralow speed (4–20 °C min^{-1}) after switching off the carbon source[19] in order to slow down the landing process to allow the CNTs to curl into serpentines. (The reason for arranging the slowly cooling step after growth is explained in the Supporting Information).

To begin with, the idea of slow cooling was validated by performing the experiment with the directions of the crystal lattice (vector **r**) and the gas flow (vector **u**) being orthogonal, that is, the angle θ is 90° (see sketch in Fig. 2a). The product was

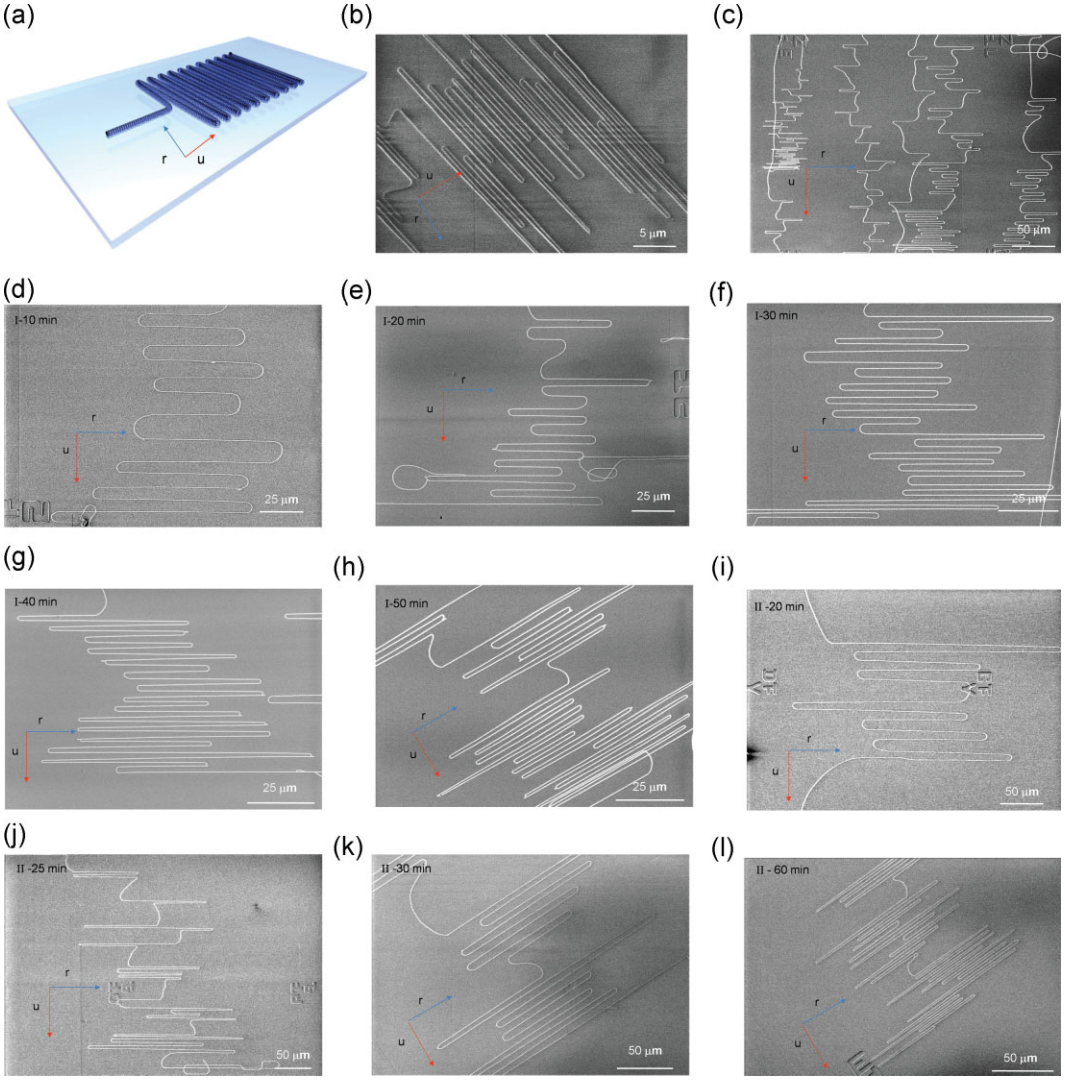

Figure 2. Serpentine CNTs with their parallel segments orthogonal to airflow. Before being annealed, the quartz substrates are patterned with markers by photolithography and wet etching to help us locate serpentine CNTs on them. a) Schematic diagram of serpentine CNTs. b) Typical SEM image of a serpentine CNT formed by slow cooling (60 min) from 975 °C to 775 °C. c) A panorama view of serpentine CNTs prepared by slow cooling (30 min) from 975 °C to 775 °C. This image was taken less than 100 μm away from the catalyst region. d–h) SEM images showing results of experiments with different cooling durations of 10, 20, 30, 40, and 50 min, respectively, from 975 °C to 775 °C. i–l) SEM images showing results of another set of experiments with cooling durations of 20, 25, 30, and 60 min, respectively, from 975 °C to 775 °C.

examined by scanning electron microscopy (SEM, Hitachi S4800 field emission, operated at 1 kV) and typical images are shown in Figure 2b and Figure S1 of the Supporting Information. In the serpentine CNT shown in Figure 2b, the length of the parallel segments is measured to be tens of micrometers, and the distance between them is about 0.5 μm, giving an ultrahigh ratio of the length of parallel segments to the distance between them of around 30–80. The increased density of parallel CNT segments is expected to boost the extreme current and improve the efficiency of ultrahigh-current CNT-based devices.[5,23–25] Furthermore, in the panorama SEM image shown in Figure 2c, it is clear that nearly all CNTs are contorted into the lattice direction. This evidence supports our prediction that slow cooling leads to an enhanced effect of F_r.

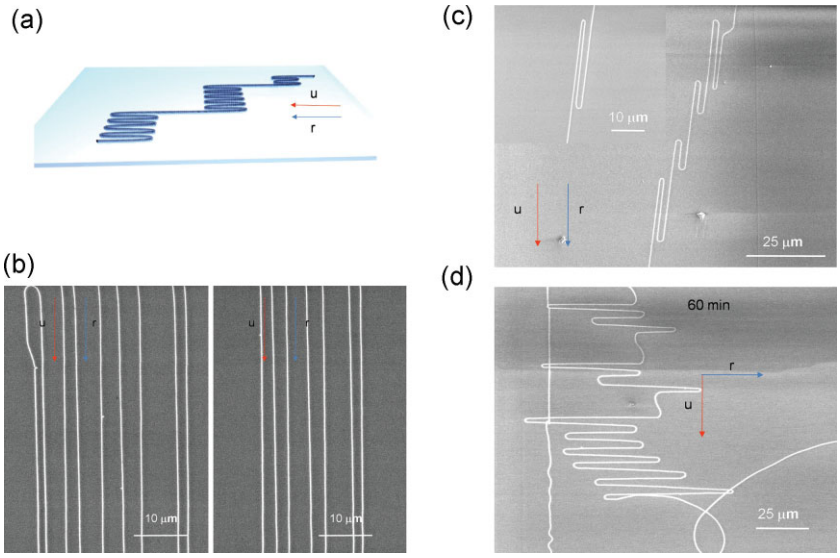

Figure 3. Effects of flow direction and flux on serpentine shape. a–c) The angle θ between r and u is about 0°. a) Sketch of serpentine CNTs. b) Two local SEM images of a serpentine CNT obtained by slow cooling (30 min) from 975 °C to 775 °C after growth. The complete SEM image of the whole serpentine CNT is provided in the Supporting Information. c) SEM image of another serpentine CNT gained through natural cooling after growth. d) SEM image of CNTs obtained with a different gas flux during slow cooling. The substrate was cooled from 975 °C to 775 °C in 60 min after growth, under an airflow of 300 sccm. $\theta = 90°$.

Sets of experiments with different cooling speed were performed to fully explore how the landing speed works on the geometry of serpentine CNTs. After the carbon source was turned off, a duration of cooling from 975 °C to 775 °C of 10, 20, 30, 40, or 50 min (Fig. 2d–h) was used. In these images, the length of parallel segments increases and the diameter of curvature decreases as the cooling duration increases. Moreover, more turns are observed at the end of each CNT, suggesting that the role of F_r is enhanced when F_u is reduced, since F_u is proportional to the length of the floating portion of CNT. Note that, to make the experimental series comparable, all experiments were performed continuously on the same batch of annealed quartz substrates within 12 h and repeated twice. Using another batch of annealed substrates, the same tendency was observed, as shown in Figure 2i–l.

Similar experiments were also performed with **r** parallel to **u** (Fig. 3a) in an attempt to broaden the application of the landing-controlled method. In Figure S2, it is clear that a CNT with longer parallel segments was obtained with slow cooling, and two portions of this CNT are displayed in Figure 3b. On the other hand, without slow cooling (after the growth stage, the furnace was unpacked to expose the sample chamber to air atmosphere to be cooled down), the number of turns within a CNT and the length of parallel segments are quite small, as shown in Figure 3c. The significant difference between Figure 3b and 3c suggests that slow cooling is favorable for F_r to influence the formation of serpentine CNTs.

In addition to the cooling speed, the directions of gas flow, and the lattice orientation, other factors that could influence F_r and F_u might also play a role in determining the geometry of serpentine CNTs, which we will address here. We found that, in order to form serpentine CNTs, the quartz substrate needs rigorous annealing. Once the crystal lattice is not formed faultlessly, the absence of F_r renders the substrate incapable of embedding the CNTs in the lattice, in which case we observed only sinuous CNTs without parallel segments along the crystal lattice (see Supporting Information), due to fluctuations of temperature or gas flow. Additional evidence was found on an isotropic surface such as a SiO_2/Si substrate (see Supporting Information). Without F_r, the most reasonable motivation for rotation of the CNTs would be air fluctuation.[26]

Generally, F_u is related to the geometry of the CNT and the condition of gas flow by (detailed analysis is given in the Supporting Information)

$$F_u = \pi \tau l d \tag{1}$$

where τ is the flow rate gradient on the surface of the CNT, l the length of the floating part of the CNT, and d the tube diameter. All of above factors have been investigated. First, we increased the flow flux during slow cooling to 300 sccm, three times the standard condition, and found the length of parallel segments greatly shortened, through comparing Figure 3d with Figure 2l (statistical data are provided in the Supporting Information). Obviously, τ increases when the flow flux increases. As a result, the increased F_u will make the landing CNT more likely to be dragged back before it can form a straight segment as long as it did.[17] That is to say, the balance point between F_r and F_u moves nearer to the center of mass of the whole serpentine CNT. Second, during the landing process, l continuously decreased, leading to a continuous decrease of F_u, which will increase the ratio of the length of parallel segments to the distances between them within one serpentine CNT (see Supporting Information). A similar phenomenon had been observed by other researchers.[27] Third, among the CNTs with different diameters, the thicker CNTs would gain shorter segments and larger radius of curvature due to increased F_u (see Supporting Information).[17,18] The larger stiffness of thicker CNTs might be another reason for the

formation of larger radii of curvature. Anyway, the tensile stress within the curved CNT was estimated to be 0.1–0.5 pN, about one order of magnitude smaller than F_u, thus unlikely to be a significant factor determining the distance between parallel segments when compared to F_u.

Based on the above evidence and analysis, it can be concluded that slow cooling from 975 °C to 775 °C is crucial for a higher percentage yield of serpentine CNTs and the formation of longer and denser parallel segments within serpentine CNTs. Through this landing-controlled method, improved parallel CNT segments arrays with identical chirality were obtained, which laid a solid basis for the manufacture of high-quality and efficient devices.

To prepare the electrical devices, the serpentine CNTs were first transferred onto SiO_2/Si substrates (Fig. 4a and its inset) by the method invented by our group.[28,29] The serpentine CNTs on quartz were first loaded onto a poly(methylmethacrylate) (PMMA) mediator, then peeled off with the mediator from the quartz, attached to the target substrate, and finally released from the mediator. The source–drain current versus gate voltage (I_{ds}–V_g) curve of the serpentine CNT shown in Figure 4b indicates an on/off ratio as high as 10^6. Although it is common for an individual CNT, such an on/off ratio could be obtained using our CNT arrays too. In Figure 4c,d, the superposition of I_{ds}–V_g and I_{ds}–V_{ds} curves of another transferred serpentine CNT also assures that all the segments within the same serpentine CNT exhibit the same properties. Besides, subthreshold swings[30] measured at two different locations (shown in Fig. 4e,f) of a newly transferred serpentine CNT are constant, as shown in Figure 4g. This is more evidence of the identical chirality of parallel segments. To further substantiate that every segment within one serpentine CNT has identical chirality, Raman spectra (Renishaw 1000, with an excitation energy of 1.96 eV (632.8 nm) and a 1 μm excitation spot size) along a serpentine CNT were recorded at nine different locations, as displayed in Figure 4h. The constant wavenumber of the radial breathing mode (RBM) and G-band also indicate that serpentine CNTs exhibit the same chirality along their length. At the same time, the absence of the D-band indicates the high quality of our product (see the Supporting Information). Based on the complete sameness of the segments from a serpentine CNT, the performance of such CNT-based devices can be easily scaled up by increasing the number of segments. Figure 4i presents the I_{ds} of serpentine CNTs as a function of the number of segments connected to the electrodes. The high linearity of the curves demonstrates that the current is proportional to the number of segments. From Figure 4c,d,g, and i, it can be deduced that, without losing the high on/off ratio exhibited by a single CNT, ultrahigh current devices up to milliampere or even higher can be produced if more segments are introduced into the devices or the distance between the electrodes is reduced.

In summary, we have shown a rational approach to crinkling ultralong CNTs into serpentine geometries by controlling the landing process. Utilizing this method, the length, density, and number of parallel CNT segments of same serpentine CNT were significantly increased. Ultrahigh-current devices with high on/off ratio based on arrays of CNTs with the same chirality were successfully built. The performance of these CNT-based devices can be easily improved by increasing the number of segments from one serpentine CNT. This controlled-landing growth of serpentine CNTs provides access to arrays of CNTs with the same

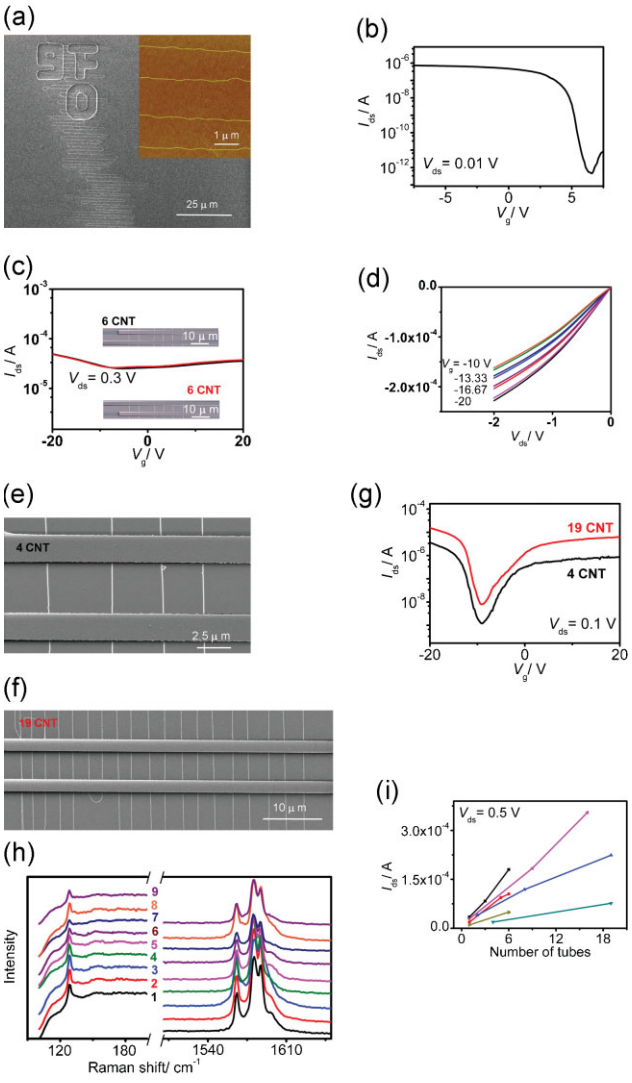

Figure 4. Transfer and electrical properties of serpentine CNTs. a) Typical SEM and atomic force microscopy (AFM, inset) images of transferred serpentine CNTs onto a silicon substrate with a 1 μm thick oxidized layer. b–i) All data were collected from transferred serpentine CNTs on a silicon substrate with an oxidized layer 1 μm (b) or 500 nm (c–i) thick. The devices consisting of multiple sections of a single serpentine CNT were fabricated by electron beam lithography (EBL) and liftoff of Pd. b) Typical I_{ds}–V_g curve of a single serpentine CNT, whose SEM image is shown in the Supporting Information. c,d) Typical I_{ds}–V_g (c) and I_{ds}–V_{ds} (d) curves measured at two different sites along another serpentine CNT. The distance between the electrodes was kept constant and the number of segments bridged by the electrodes was six in each case. Insets: SEM images around the electrodes. e,f) SEM images around electrodes at two different sites along a new serpentine CNT. The distance between the electrodes was kept constant and the numbers of segments bridged by the electrodes were 4 and 19. g) Typical I_{ds}–V_g curves measured using the sites shown in (e) and (f). The subthreshold swings of the two curves in (g) are 1260 and 1310 mV decade^{-1}, respectively. h) Typical Raman spectra collected at 9 different sites along a different serpentine CNT. The SEM images around the first 8 sites are provided in the Supporting Information, while the last site was at another point on the same serpentine CNT for comparison. i) I_{ds} of 6 different serpentine CNTs as a function of the number of CNTs bridged by the electrodes. The channel length of the electrode is 2–4 μm and it is constant for the same serpentine CNT.

chirality and will broaden CNT application in various nanodevices.

Experimental

Annealing Processes: The quartz substrates were annealed in a muffle furnace (Pyramid TXCS6-II). In the annealing processes, the quartz substrates were heated to 900 °C within 1 h, then kept at 900 °C for 8 h and finally cooled down to room temperature naturally or under temperature programming.

Standard Growth Processes: Serpentine CNTs were synthesized using methane as the carbon source and Fe as a catalyst on ST-cut annealed quartz substrates. To start the growth, a catalyst solution (0.01 M) was applied to one edge of a quartz substrate by microcontact printing. The substrate with catalyst precursor was then placed in a horizontal 3.7 cm quartz tube furnace with the catalyst end facing the gas flow, then the catalyst was heated at 700 °C for 10 min to oxidize the catalyst, the temperature was increased to 975 °C in an Ar environment, the catalyst was prereduced at 975 °C in H_2 (200 sccm) for 10 min, and then a flow of CH_4 (40 sccm) and H_2 (60 sccm) was introduced into the furnace at 975 °C for 30 min. Finally, the reactor was purged in a flow of Ar (40 sccm) and H_2 (60 sccm) in a slow cooling step from 975 °C to 775 °C with variable time for the formation of serpentine CNTs and then cooled down to room temperature.

Characterization: Before annealing the quartz, we made the patterned markers by photolithography and wet etching to locate serpentine CNTs on them. That makes it convenient for us to recognize and address any serpentine CNT on the surface. A scanning electron microscope (Hitachi S4800 field emission, Japan), a micro-Raman spectrometer (Renishaw 1000) assembled with a confocal imaging microscope, with an excitation energy of 1.96 eV (632.8 nm) and a 1 μm excitation spot size, and an atomic force microscope (Veeco NanoScope III, Veeco Co., USA, operated in tapping mode) were used to characterize the as-produced serpentine CNTs.

Electrical Characterization: For the electrical characterization, serpentine CNTs were transferred onto a silicon substrate with a 500 nm or 1 μm thick oxidized layer. The serpentine CNTs on quartz were first loaded onto a PMMA mediator, then peeled off with the mediator from the quartz, attached to the target substrate, and finally released from the mediator. PMMA, due to its low viscosity and good wetting capability, can conform well to the product on source substrates and hence keep the original shape of serpentine CNTs as much as possible. Besides, the easily solubility of PMMA in many organic solvents makes the target substrates very clean after transfer. This enhances the quality of the devices built from these transferred materials. The devices consisting of multiple sections of a single serpentine CNT are fabricated by electron beam lithography and liftoff of Pd.

Acknowledgements

Y. G. Yao and X. C. Dai contributed equally to this work. This work was supported by NSFC (20828004, 20725307, and 50821061) and MOST (2006CB932701, 2006CB932403, and 2007CB936203). Y.G.Y. acknowledges Mr. X. F. Song and Mr. Y. Z. Wang from Peking University for their great help at EBL. We also thank B. Zhang, K. Yan, and T. Gao for useful discussions. Supporting Information is available online from Wiley InterScience or from the authors.

Received: April 14, 2009
Revised: May 21, 2009
Published online: August 3, 2009

[1] P. Avouris, Z. H. Chen, V. Perebeinos, *Nat. Nanotechnol.* **2007**, *2*, 605.
[2] R. H. Baughman, A. A. Zakhidov, W. A. de Heer, *Science* **2002**, *297*, 787.
[3] P. L. McEuen, *Nature* **1998**, *393*, 15.
[4] Y. Yao, C. Feng, J. Zhang, Z. Liu, *Nano Lett.* **2009**, *9*, 1673.
[5] L. Ding, A. Tselev, J. Y. Wang, D. N. Yuan, H. B. Chu, T. P. McNicholas, Y. Li, J. Liu, *Nano Lett.* **2009**, *9*, 800.
[6] B. Wang, C. H. P. Poa, L. Wei, L. J. Li, Y. H. Yang, Y. Chen, *J. Am. Chem. Soc.* **2007**, *129*, 9014.
[7] Z. F. Ren, *Nat. Nanotechnol.* **2007**, *2*, 17.
[8] R. E. Smalley, Y. B. Li, V. C. Moore, B. K. Price, R. Colorado, H. K. Schmidt, R. H. Hauge, A. R. Barron, J. M. Tour, *J. Am. Chem. Soc.* **2006**, *128*, 15824.
[9] S. Reich, L. Li, J. Robertson, *Chem. Phys. Lett.* **2006**, *421*, 469.
[10] G. Lolli, L. A. Zhang, L. Balzano, N. Sakulchaicharoen, Y. Q. Tan, D. E. Resasco, *J. Phys. Chem. B* **2006**, *110*, 2108.
[11] M. Zheng, E. D. Semke, *J. Am. Chem. Soc* **2007**, *129*, 6084.
[12] X. L. Li, X. M. Tu, S. Zaric, K. Welsher, W. S. Seo, W. Zhao, H. J. Dai, *J. Am. Chem. Soc.* **2007**, *129*, 15770.
[13] S. Campidelli, M. Meneghetti, M. Prato, *Small* **2007**, *3*, 1672.
[14] G. Y. Zhang, P. F. Qi, X. R. Wang, Y. R. Lu, X. L. Li, R. Tu, S. Bangsaruntip, D. Mann, L. Zhang, H. J. Dai, *Science* **2006**, *314*, 974.
[15] H. J. Huang, R. Maruyama, K. Noda, H. Kajiura, K. Kadono, *J. Phys. Chem. B* **2006**, *110*, 7316.
[16] M. S. Arnold, A. A. Green, J. F. Hulvat, S. I. Stupp, M. C. Hersam, *Nat. Nanotechnol.* **2006**, *1*, 60.
[17] N. Geblinger, A. Ismach, E. Joselevich, *Nat. Nanotechnol.* **2008**, *3*, 195.
[18] S. Jeon, C. G. Lee, J. Y. Tang, J. Hone, C. Nuckolls, *Nano Res.* **2008**, *1*, 427.
[19] M. Hofmann, D. Nezich, A. Reina, J. Kong, *Nano Lett.* **2008**, *12*, 4122.
[20] S. M. Huang, M. Woodson, R. Smalley, J. Liu, *Nano Lett.* **2004**, *4*, 1025.
[21] Z. Jin, H. B. Chu, J. Y. Wang, J. X. Hong, W. C. Tan, Y. Li, *Nano Lett.* **2007**, *7*, 2073.
[22] Y. G. Yao, Q. W. Li, J. Zhang, R. Liu, L. Y. Jiao, Y. T. Zhu, Z. F. Liu, *Nat. Mater.* **2007**, *6*, 283.
[23] K. Ryu, A. Badmaev, C. Wang, A. Lin, N. Patil, L. Gomez, A. Kumar, S. Mitra, H. S. P. Wong, C. W. Zhou, *Nano Lett.* **2009**, *9*, 189.
[24] S. J. Kang, C. Kocabas, T. Ozel, M. Shim, N. Pimparkar, M. A. Alam, S. V. Rotkin, J. A. Rogers, *Nat. Nanotechnol.* **2007**, *2*, 230.
[25] X. L. Li, L. Zhang, X. R. Wang, I. Shimoyama, X. M. Sun, W. S. Seo, H. J. Dai, *J. Am. Chem. Soc.* **2007**, *129*, 4890.
[26] B. H. Hong, J. Y. Lee, T. Beetz, Y. M. Zhu, P. Kim, K. S. Kim, *J. Am. Chem. Soc.* **2005**, *127*, 15336.
[27] J. Huang, W. Choi, *Nanotechnology* **2008**, *19*, 505601.
[28] L. Y. Jiao, X. J. Xian, Z. Y. Wu, J. Zhang, Z. F. Liu, *Nano Lett.* **2009**, *9*, 205.
[29] L. Y. Jiao, B. Fan, X. J. Xian, Z. Y. Wu, J. Zhang, Z. F. Liu, *J. Am. Chem. Soc.* **2008**, *130*, 12612.
[30] S. Pisana, C. Zhang, C. Ducati, S. Hofmann, J. Robertson, *IEEE Trans. Nanotechnol.* **2008**, *7*, 458.